Dong, B., Jiang, C., Liu, X., Deng, Y., & Huang, L. (2020). Theoretical characterization and modal directivity investigation of the interaction noise for a small contra-rotating fan. *Mechanical Systems and Signal Processing*, 135, 106362.
doi: https://doi.org/10.1016/j.ymssp.2019.106362

Theoretical Characterization and Modal Directivity Investigation of the Interaction Noise for a Small Contra-Rotating Fan

Bin Dong[a,b,c],
Changyong Jiang[a,c,*],
Xiang Liu[a,c],
Yi Deng[d]
Lixi Huang[a,c]

[a]Department of Mechanical Engineering, The University of Hong Kong, Pokfulam Road, Hong Kong SAR, China.

[b]High Speed Aerodynamics Institute, China Aerodynamics Research and Development Center, No.6, South Section, Second Ring Road, Mianyang, Sichuan, China, 621000.

[c]Laboratory for Aerodynamics and Acoustics, Zhejiang Institute of Research and Innovation, The University of Hong Kong, Hong Kong SAR, China.

[d]School of Chemical Engineering, Sichuan University, Chengdu, Sichuan, China, 610065

Corresponding author: Changyong Jiang, Department of Mechanical Engineering, The University of Hong Kong, Pokfulam Road, Hong Kong SAR, China.
E-mail: jiangchangyong1991@connect.hku.hk

Submitted to Mechanical Systems and Signal Processing April 24 2019
Accepted September 7 2019

Author Biographies

Bin Dong was once a PhD student at the University of Hong Kong. His research interests are in aerodynamic noise and fluid dynamics.

Changyong Jiang,

Xiang Liu,

Yi Deng,

Lixi Huang,

Theoretical Characterization and Modal Directivity Investigation of the Interaction Noise for a Small Contra-Rotating Fan

Abstract:

The interaction noise radiated from **c**ontra-**r**otating (CR) fans is theoretically characterized, focusing on the unsteady lift force caused by the aerodynamic interaction between the front and rear rotors. In the formulation, blade section misalignments leading to blade sweep and lean are considered. It is demonstrated that the conventional stator-rotor interaction noise problem is a special case of the present model, whereas the rotor-stator case is not. Modal directivities of lower-order interaction tones are investigated with the derived formula, which is generally validated by the experimental results. For extracting the interaction tones from the measured acoustic data, the Vold-Kalman filter is applied, with which the influences of broadband noise are excluded. It is found that the modal directivity of interaction noise for CR fans is more complicated than that for conventional fans. Theoretically, the leading order thrust noise is found to peak along the rotation axis and plummet in the rotational plane. For the first-order mode, the predicted directivity exhibits a forward-leaning characteristic, which is in good agreement with the experimental result. The predicted directivity patterns of second- and third-order modes are dominated by the drag noise component and peak in the direction near the rotational plane.

(196 words)

Keywords: contra-rotating fan; interaction noise characterization; modal directivity; Vold-Kalman filter.

Nomenclature

a	= empirical wake parameter	U_{in}	= incident velocity, m/s
B_i	= rotor blade number	U_0, U_r	= mean flow velocity, m/s
b_w	= half-wake width, m	V	= vane or strut number
c_i	= blade chord length, m	w_p	= amplitude of the p-th harmonic, m/s
c_0	= speed of sound, m/s	$w(\xi_1,\xi_2)$	= velocity deficit profile, m/s

d_i = blade space, m

f_n, f_{m_1,m_2} = interaction frequency, Hz

f_i = blade passing frequency, Hz

F = lift force, N/m

F_w = response factor, N/m

f_{D}^{l} = drag force, N/m^2

f_{T}^{l} = thrust force, N/m^2

f_{D}^{*} = net drag force, N/m^2

f_{T}^{*} = net thrust force, N/m^2

$J_m(z)$ = Bessel function of first kind

k_n, k_{m_1,m_2} = wavenumber, /m

l = blade index, integer

m = circumferential mode order

m_1, m_2 = integer

M = rotational Mach number at a radius of r

M_r = Mach number, U_r/c_0

M_t = tip rotational Mach number

n, q = integer

p = integer, m_1B_1

P = sound pressure, Pa

r = radius of blade section, m

r_e = typical radius, m

r_h = blade hub radius, m

r_t = blade tip radius, m

R_0 = source to observer distance, m

$S_c(\sigma_p, M_r)$ = Sears' function

T = large time interval, s

$w(\xi_1)$ = wake centerline velocity deficit, m/s

w_2^{ζ} = upwash velocity of wakes, m/s

$W(p)$ = wavenumber spectrum of wake deficit

(x_1,x_2,x_3) = absolute frame of reference

(y_1,y_2,y_3) = moving frame fixed to source

r,φ,y_1 = cylindrical coordinates of source

r_o,θ,φ_o = spherical coordinates of observer

(ξ_1,ξ_2) = frame fixed to a front blade at a radius of r

(ζ_1,ζ_2) = frame fixed to a rear blade at a radius of r

χ = blade stagger angle, deg

φ_w = phase shift due to $\Delta\xi$, rad

φ_b = phase shift due to $\Delta\zeta$, rad

δ = Kronecker delta function

η_h = axial rotor-rotor gap on the hub, m

μ = $\chi_1+\chi_2$, deg

ν = $k_n r_e$

ρ_0 = density, kg/m^3

σ_p = reduced frequency

τ = source time, s

$\Delta\xi$ = front blade section misalignments, m

$\Delta\zeta$ = rear blade section misalignments, m

Ω = angular velocity, rad/s

Ω_e = $\Omega_1+\Omega_2$, rad/s

Subscripts

1 = quantities related to the front rotor

2 = quantities related to the rear rotor

1 Introduction

The concept of **c**ontra-**r**otating (CR) configurations has been investigated experimentally and theoretically since the 1940s [1, 2], ranging from turbomachinery components like propellers, compressors, and turbines in the aviation industry, to small scale devices such as computer cooling

fans and building ventilation fans in daily situations. In the 1970s and 1980s, this concept was further studied for aircraft propulsion systems due to its potential for higher efficiency and less fuel consumption [3, 4].

However, a thorny problem arising for the CR propulsion system (e.g., CR propellers) is that it generates very high noise levels due to the strong interaction between the front and rear rotors. It is imaginable that the interaction noise would pose significant discomfort to passengers inside the aircraft cabin. In order to tackle this problem, researchers made many efforts to explain noise radiation mechanisms of CR configurations in the 1980s. Applying Lighthill's acoustic analogy [5] to propellers, Hanson [6] established a frequency domain method to interpret the noise radiated from CR propellers, and classified interaction effects between propeller rows into acoustic interference and aerodynamic interference. Parry [7] developed a theoretical model to predict the tonal noise generated by CR propellers through asymptotic approximation techniques. Besides, amounts of experimental work were also conducted other than theoretical work. Parametric studies on CR propellers were performed by Fujii et al. [8] and Metzger and Brown [9] to better understand how the radiated sound could be affected by varying propeller tip speeds and changing propeller row spacing. Woodward [10] conducted experiments for a high-speed CR propeller at a Mach number of 0.2, which was the simulated velocity condition of airplane takeoff and approach, to investigate the directivity characteristics of rotor-alone tones and interaction tones. The experimental results demonstrated that the first order rotor-alone tone presented highest sound pressure level (SPL) near the propeller plane while interaction tones played a role throughout the sideline and became stronger toward the rotation axis. In addition, the interaction tone levels were sensitive to propeller row spacing, whereas rotor-alone tones exhibited no spacing effects. The rotor wake and vortex flow field of a CR unducted fan were systematically studied in a scale model with three-dimensional (3D) hot-wire anemometry by Shin et al. [11]. In their work, a set of benchmark aerodynamic data of the rotor wake and vortex structure were provided for a CR fan, which could be related to its acoustic signature.

In the new century, more efforts have been made in the characterization and reduction of noise from CR propulsion system, as it remained challenging to suppress noise emissions from CR propeller engines without sacrificing propulsive efficiency. Aerospace companies made a lot of efforts to construct the design process and test rig of CR configurations, with support of

governments, research institutes, and academia [12]. Schnell [13] investigated the blade pressure fluctuations of a CR turbofan experimentally and numerically. It was concluded that the blade pressure fluctuations were mainly caused by upstream shedding wakes. The concept of CR low-speed fan was applied for a high bypass ratio engine in SNECMA [14]. In their work, a scale model of CR fan was aerodynamically and mechanically designed with a multi-objective optimization strategy based on an evolutionary algorithm, where noise reduction of 6dB was reported.

For the purpose of predicting the broadband rotor-wake interaction noise and the broadband rotor trailing edge noise, Blandeau [15] developed two fast semi-analytical models, which exhibited good agreements with noise measurements from a scale model of a CR open rotor. Recent results from NASA for validating an open rotor noise prediction code were summarized by Envia [16], which was based on a high-blade-count asymptotic approximation to the Ffowcs Williams and Hawkings (FW-H) equation [17]. It was found that the noise trends were reasonably predicted, whereas predicting the absolute noise levels was challenging. Following the model established by Blake [18], a general formula was derived by Wang and Huang [19] for predicting the far-field interaction noise from small CR fans. Effects of the interstage gap were experimentally studied, and it was found that when the nondimensional interstage gap is lower than 0.41, the far-field sound pressure level (SPL) tends to follow an exponential decay law with the interstage gap, implying an exponential decay of 3D rotor wake as well.

The current study is mainly focused on deriving a new formulation approach, based on the model of Goldstein [20], to characterize the interaction noise of CR fans. It is believed that the interaction noise is due to unsteady lift force acting on rear rotor blades; therefore, the formulation is started from accounting for the aerodynamic interaction between rotors. In the previous literature, the aerodynamic interaction between spatially nonuniform flow and a single rotating blade is well quantified by Goldstein [20], and Blake [18] further solved the problem of a rotor response to an upstream stator. Here, we extend their analyses into CR fans. Specifically, because the front and rear rotors in CR fans are rotating in reverse directions, the aerodynamic interaction modeling occurs in the time domain, where the effects of blade sweep as well as lean arising from blade section misalignments are considered. We hope that the modeling of aerodynamic interaction may help the enhancement of understanding the underlying mechanisms of interaction noise in CR fans. The acoustic analysis of interaction noise is then facilitated using the result from the aerodynamic

analysis. Ultimately, a frequency domain formula, which describes the far-field noise radiation of CR fans, is given. Based on the derived formula, the difference in modal directivity patterns between CR fans and conventional fans is pointed out. As an example of further application, the modal directivity of the radiated interaction noise from a small CR fan is investigated, which is experimentally validated. The derived formula is intended to help develop quieter CR fans or devise noise control methods to existing CR fans.

2 Theoretical characterization of interaction noise

In this section, the formulation of the interaction noise radiated from CR fans is provided. In essence, the noise is emitted from rear rotor blades, where the unsteady lift force F exerts and varies with time. This results in a fluctuating pressure P that is in proportion to $\partial F/\partial \tau$. The amplitude of F is associated with the incidence angle of the incoming flow, which is strongly influenced by a passing vortex. The turbulent wakes shed from the blade trailing edge of the front rotor impinges on the blade leading edge of the rear rotor, generating stochastic changes in the incidence angle, which would induce F and hence the interaction noise.

2.1 Aerodynamic interaction between rotors

To quantify the interaction noise, the unsteady lift force F generated from the aerodynamic interaction between rotors should be predetermined. The methods to quantifying F is based on thin airfoil theory [20], which gives a linear relationship between the lift force per unit span and the upwash velocity. For two CR blade rows, as wakes from the front blade row pass by and impinge on the rear blade row, the rear blades experience the wake velocity deficit periodically. This will give rise to an upwash velocity relative to the rear blades and thus the unsteady force F. Fig. 1 shows two arrays of blade sections, unrolled at a radial position r. As for the rear rotor rotating at an angular velocity of Ω_2, B_2 blades with stagger angle χ_2 are evenly distributed, which interact with the wakes from B_1 uniformly spaced blades with stagger angle χ_1. The front rotor rotates reversely at Ω_1, which is not necessarily equal to Ω_2. The blade spaces for the front and rear rotors are $d_1 = 2\pi r/B_1$ and $d_2 = 2\pi r/B_2$, respectively. η_h is the axial separation gap between the mid-chord disks of the two rotors on the hub. Two coordinate systems ξ_1-ξ_2 and ζ_1-ζ_2 are defined with their origins located at the associated mid-chord points. Coordinate offsets $\Delta\xi_i$ and $\Delta\zeta_i$ account for blade section misalignments at r relative to the sections on the hub, with subscripts $i = 1$ and 2 denoting

the chordwise and normal directions, respectively. In the ξ_1-ξ_2 system, the fluid just out of the wake is thought to leave the front blade row in the ξ_1-direction with a velocity of U_0. On the other hand, in the ζ_1-ζ_2 system, the wake relative to a rear blade has a mean velocity of U_r in the ζ_1-direction, which is essentially the resultant velocity of U_0 and $(\Omega_1+\Omega_2)r$, as demonstrated in Fig. 1.

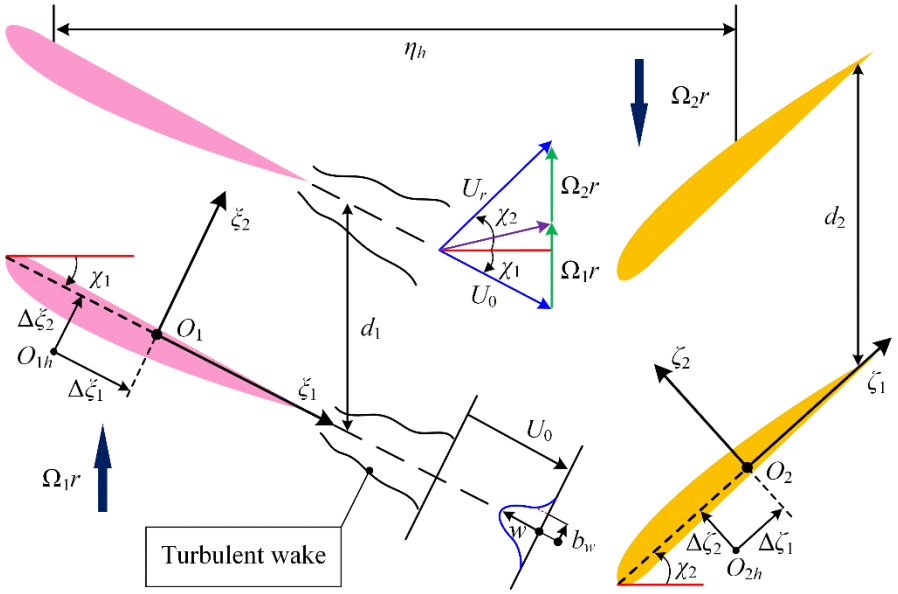

Fig. 1. Two-dimensional illustration of the aerodynamic interaction between rotors.

It is assumed in the ξ_1-ξ_2 system that the incoming flow outside the front blade row consists of a steady part U_0 and a small spatially varying part w, which only changes in the ξ_2-direction. As is similar to the derivation of Goldstein, the problem is thought to be linear, and it is only necessary to consider a single harmonic component of the spatially nonuniform part w [20]. Thus, the incident velocity U_{in} can be written as

$$U_{in} = U_0 - w_p e^{ip\varphi_\xi}, \tag{1}$$

where w_p is the amplitude of the p-th harmonic component and φ_ξ is the angular coordinate in the ξ_1-ξ_2 system, defined as

$$\varphi_\xi = \frac{\xi_2 + \Delta\xi_2}{r\cos\chi_1}. \tag{2}$$

As given in Fig. 1, the ζ_1-ζ_2 system is rotated away from the ξ_1-ξ_2 system with an angle of $\mu = \chi_1+\chi_2$. In a time τ, the ξ_1-ξ_2 system would translate a distance of $(\Omega_1+\Omega_2)r\tau\cos\chi_1$ in the ξ_2-direction. Hence, relative to a particular rear blade (say, blade I), performing coordinate transformation and including blade section misalignments yield

$$\xi_2 + \Delta\xi_2 = (\zeta_1 + \Delta\zeta_1)\sin\mu + (\zeta_2 + \Delta\zeta_2)\cos\mu - (\Omega_1 + \Omega_2)r\tau\cos\chi_1, \tag{3}$$

which could be used to relate coordinates in the ζ_1-ζ_2 system to the angular coordinate in the ξ_1-ξ_2 system. The amplitude w_p at r can be calculated from the spatially varying part $w(r,\varphi_\xi)$ as

$$w_p = w(p,r) = \frac{1}{2\pi}\int_0^{2\pi} w(r,\varphi_\xi)e^{-ip\varphi_\xi}d\varphi_\xi = \left|w(p,r)\right|e^{ip\varphi_w}, \tag{4}$$

where the angle φ_w accounts for the phase delay of the upstream wake due to blade section misalignments of the front blade and can be described as

$$\varphi_w = \Delta\xi_2/(r\cos\chi_1). \tag{5}$$

The profile of each wake at radius r is assumed to repeat identically in the circumferential direction and can be approximated as a Gaussian function [18],

$$w(r,\xi_1,\xi_2) = w(\xi_1)\exp(-a(\xi_2/b_w)^2), \tag{6}$$

where $w(\xi_1)$ is the wake centerline velocity deficit, b_w is the half-wake width, and a is an empirical wake parameter. For B_1 front blades, φ_ξ can be related to the coordinate ξ_2 by

$$\xi_2 = \left(\varphi_\xi - \varphi_w - 2\pi j/B_1\right)r\cos\chi_1, \tag{7}$$

where the index j is an integer in the range of [1, B_1]. Then, using Eqs. (6) and (7), a continuous nonuniform velocity function arising from the pulse train of B_1 upstream wakes can be obtained

$$w(r,\varphi) = w(\xi_1)\sum_{j=1}^{B_1}\exp\left\{-\frac{a}{b_w^2}\left[\left(\varphi_\xi - \varphi_w - 2\pi j/B_1\right)r\cos\chi_1\right]^2\right\}. \tag{8}$$

Note that the Gaussian model applies only to thin wakes. If wake width $2b_w$ is not small compared to the blade space d_1, the overlap between adjacent wakes will occur. In that case, mutual blade effects cannot be neglected, and the model becomes invalid. In the current study, the problem is limited to thin wakes. To find the circumferential harmonics concerning a particular blade of reference, we restrict φ in an angular sector [$-c_1/2r$, $c_1/2r$], with c_1 being the chord length of the front blade. Inserting Eqs. (7) and (8) into Eq. (4), utilizing integral transformation from φ to ξ_2 and carrying out Poisson summation over j, for the p-th harmonic component, we get

$$w(p,r) = w(\xi_1)\sum_{m_1=-\infty}^{\infty} e^{ip\varphi_w}\frac{B_1}{2\pi r\cos\chi_1}\int_{-c_1/2}^{c_1/2} e^{-a(\xi_2/b_w)^2}e^{-ip\xi_2/(r\cos\chi_1)}d\xi_2\delta(p - m_1B_1). \tag{9}$$

For thin wakes, limits of the integral can be safely extended to infinite; therefore, a closed-form integration can be obtained according to the integral tables in Ref. [21]

$$w(p,r) = w(\xi_1)B_1 \sum_{m_1=-\infty}^{\infty} W(p)\delta(p - m_1 B_1)e^{ip\varphi_w}\,, \tag{10}$$

where the wavenumber spectrum of the wake deficit is given by

$$W(p) = \frac{b_w}{2\pi r\cos\chi_1}\sqrt{\frac{\pi}{a}}\exp\left[-\frac{1}{a}\left(\frac{pb_w}{2r\cos\chi_1}\right)^2\right]. \tag{11}$$

Equation (11) suggests that the energy of the wake deficit also follows a Gaussian distribution that concentrates around $m_1 = 0$. With Eqs. (2), (3) and (10), and considering the velocity relationship of $(\Omega_1+\Omega_2)r/\sin\mu = U_r/\cos\chi_1$, Eq. (1) can be rewritten as

$$U_i = U_0 - w(p,r)\exp\left[-\mathrm{i}p(\Omega_1+\Omega_2)\left(\tau - \frac{\zeta_1+\zeta_2\cot\mu}{U_r} - \frac{\Delta\zeta_1+\Delta\zeta_2\cot\mu}{U_r}\right)\right]. \tag{12}$$

The time-varying term of Eq. (12) would produce two unsteady velocity components in the ζ_1-ζ_2 system. The upwash velocity in the ζ_2-direction w_2^{ζ} is responsible for generating the unsteady lift force F that acts on the rear blade,

$$w_2^{\zeta} = w(\xi_1)\sin\mu B_1 \sum_{m_1=-\infty}^{\infty} W(p)\delta(p - m_1 B_1)e^{ip(\varphi_w+\varphi_b)}\exp\left[\mathrm{i}\left(k_1(\zeta_1 - U_r\tau) + k_2\zeta_2\right)\right], \tag{13}$$

where

$$\begin{cases} k_1 = (\Omega_1+\Omega_2)\dfrac{p}{U_r} \\ k_2 = k_1\cot\mu \\ \varphi_b = (\Omega_1+\Omega_2)\dfrac{\Delta\zeta_1+\Delta\zeta_2\cot\mu}{U_r} \end{cases}, \tag{14}$$

and φ_b explains the phase delay due to blade section misalignments in the rear blade. Using two-dimensional (2D) compressible Sears' function [20], that is, $S_c(\sigma_p, M_r)$, F can be quantified as

$$F = F_w B_1 \sum_{m_1=-\infty}^{\infty} W_p S_c(\sigma_p, M_r)e^{ip(\varphi_w+\varphi_b)}e^{-ip(\Omega_1+\Omega_2)\tau}\delta(p - m_1 B_1)\,, \tag{15}$$

where F_w is defined as a response factor,

$$F_w = \pi c_2 \rho_0 U_r w(\xi_1)\sin\mu\,. \tag{16}$$

Within the 2D Sears function, M_r is the Mach number of the velocity U_r, namely $M_r = U_r/c_0$ (c_0 is the speed of sound), and σ_p is the so-called reduced frequency, defined as

$$\sigma_p = \frac{k_1 c_2}{2} = \frac{p(\Omega_1 + \Omega_2)c_2}{2U_r}\,. \tag{17}$$

Equations (15) to (17) indicate that the force F is periodic in time with a fundamental frequency of $\Omega_e = \Omega_1+\Omega_2$, and that the p-th harmonic of F is solely determined by the p-th spatial harmonic of the incoming flow. It should be noted that, with $\Omega_1 = 0$, Eq. (15) applies to the stator-rotor interaction problem, where the reduced frequency is solely determined by Ω_2. Hence, it is clear that the stator-rotor interaction problem is a particular case of the rotor-rotor interaction problem. In addition, Eq. (15) merely accounts for the force acting on a specific blade of the rear rotor (blade I). The solution for another blade (say, blade l with $1 \le l \le B_2$), can be easily found as follows. Let index l be counted in the direction against Ω_2. Since there are B_2 evenly spaced blades, blade l would behave like blade I leaning in the circumferential direction by an angular difference of $-2\pi(l-1)/B_2$. Note that for an observer in the absolute frame, the force acting on blade I at time τ is the same as the force acting at the time $\tau+2\pi(l-1)/(\Omega_2 B_2)$ on blade l, so the force exerting on the l-th blade can be evaluated as

$$F = F_w B_1 \sum_{m_1=-\infty}^{\infty} W_p S_c(\sigma_p, M_r) e^{\mathrm{i}p(\varphi_w+\varphi_b)} e^{-\mathrm{i}p(\Omega_1+\Omega_2)(\tau+2\pi(l-1)/B_2\Omega_2)} e^{\mathrm{i}p2\pi(l-1)/B_2} \delta(p - m_1 B_1)\,. \tag{18}$$

2.2 Interaction noise in the far-field

The formulation of the interaction noise for CR fans begins with the model of Goldstein, which predicts far-field noise radiation due to the interaction between unsteady inflow and the rotor. Note that the chordwise blade noncompactness is assumed negligible and therefore the acoustic source is regarded as being concentrated in the rotational plane of the rear rotor. The predicted radiated sound pressure P is expressed as [20]

$$\begin{aligned} P = \frac{\mathrm{i}k_n}{4\pi r_o} e^{\mathrm{i}k_n r_o} \sum_{m=-\infty}^{\infty} e^{\mathrm{i}m(\varphi_o-\pi/2)} \int_A J_m(k_n r \sin\theta) e^{-\mathrm{i}m\varphi} \\ \times \left[\cos\theta \left(\frac{\Omega_2}{2\pi} \int_0^{\frac{2\pi}{\Omega_2}} e^{\mathrm{i}(n-m)\Omega_2\tau} f_{\mathrm{T}}^*(r,\varphi,\tau) d\tau \right) \right. \\ \left. - \frac{m}{k_n r} \left(\frac{\Omega_2}{2\pi} \int_0^{\frac{2\pi}{\Omega_2}} e^{\mathrm{i}(n-m)\Omega_2\tau} f_{\mathrm{D}}^*(r,\varphi,\tau) d\tau \right) \right] r d\varphi dr \end{aligned}\,, \tag{19}$$

where, the domain of integration A is the blade cross-sectional area; (r_o, θ, φ_o) are the spherical coordinates for the far-field observer; (r, φ, y_1) are the cylindrical coordinates for the rotating

source; f_T^* and f_D^* are the net thrust and drag forces per unit area, respectively; ρ_0 is the density of steady background flow; $k_n = n\Omega_2/c_0$ is the wavenumber of the n-th harmonic of Ω_2. The geometric parameters in Eq. (19) are shown in Fig. 2. The y-coordinate system is fixed to the rear blade with the y_1-axis perpendicular to the rotational plane, and the x-coordinate system is the absolute reference frame.

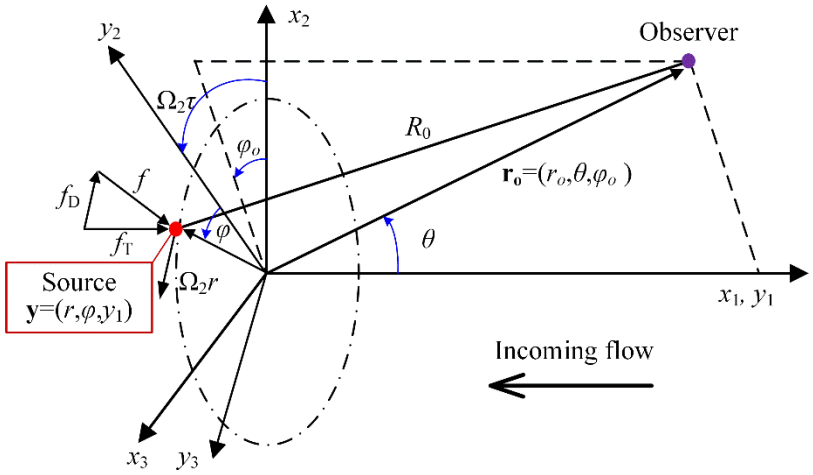

Fig. 2. Coordinate systems for noise source and observer.

The unsteady force components acting on blade I at time τ are denoted by $f_\alpha^1(r,\varphi,\tau)$, with subscripts α = T and D indicating the thrust and drag forces, respectively. The angle φ of the source in the y-coordinate system is limited in an angular sector $[-c_2/2r, c_2/2r]$, with c_2 being the chord length of the rear blade. It has been stated that the force acting on blade I at time τ is the same as the force acting at the time $\tau+2\pi(l-1)/(\Omega_2 B_2)$ on blade l, so the force on the l-th blade takes the form

$$f_\alpha^l = f_\alpha^1\left[r, \varphi - 2\pi(l-1)/B_2, \tau + 2\pi(l-1)/(\Omega_2 B_2)\right]. \tag{20}$$

Then, we have

$$f_\alpha^* = \sum_{l=1}^{B_2} f_\alpha^l. \tag{21}$$

Note that it is also possible to stipulate that the force acting on blade 1 at time τ is the same as the force acting at the time $\tau-2\pi(l-1)/(\Omega_2 B_2)$ on blade l that is displaced from blade 1 by an angle difference of $2\pi(l-1)/B_2$. These two stipulations are equivalent and therefore make no difference

to the results. Substituting Eqs. (20) and (21) into Eq. (19) and collecting like terms, the radiated pressure P can be further expressed as

$$\begin{aligned} P = & \frac{\mathrm{i}k_n}{4\pi r_o} e^{\mathrm{i}k_n r_o} \sum_{m=-\infty}^{\infty} \sum_{l=1}^{B_2} e^{\mathrm{i}m(\varphi_o - \pi/2)} \frac{\Omega_2}{2\pi} \int_0^{\frac{2\pi}{\Omega_2}} e^{\mathrm{i}(n-m)\Omega_2 \tau} e^{\mathrm{i}2\pi n(l-1)/B_2} d\tau \\ & \times \int_{r_h}^{r_t} J_m(k_n r \sin\theta) \left(\cos\theta \int f_{\mathrm{T}}^l e^{-\mathrm{i}m\varphi} r d\varphi - \frac{m}{k_n r_s} \int f_{\mathrm{D}}^l e^{-\mathrm{i}m\varphi} r d\varphi \right) dr \end{aligned}, \tag{22}$$

where r_h and r_t are the hub radius and the tip radius, respectively. It should be noted that the result of the integral $\int f_\alpha^l e^{-\mathrm{i}m\varphi} r d\varphi$ (α = T or D) is the unsteady force (thrust or drag) per unit span, which has been predetermined in Sec. 2.1. Therefore, upon referring to Eq. (18), the thrust and drag forces per unit span of blade l can be respectively determined as

$$\int f_{\mathrm{T}}^l e^{-\mathrm{i}m\varphi} r d\varphi = F \sin\chi_2 , \tag{23}$$

and

$$\int f_{\mathrm{D}}^l e^{-\mathrm{i}m\varphi} r d\varphi = F \cos\chi_2 . \tag{24}$$

Inserting Eqs. (23) and (24) into Eq. (22), we have

$$\begin{aligned} P = & \frac{\mathrm{i}B_1 k_n}{4\pi r_o} e^{\mathrm{i}k_n r_o} \sum_{m=-\infty}^{\infty} \sum_{m_1=-\infty}^{\infty} e^{\mathrm{i}m(\varphi_o - \pi/2)} \left[\sum_{l=1}^{B_2} e^{\mathrm{i}(n+p-p(\Omega_1+\Omega_2)/\Omega_2)2\pi(l-1)/B_2} \right] \\ & \times \left\{ \frac{\Omega_2}{2\pi} \int_0^{\frac{2\pi}{\Omega_2}} e^{\mathrm{i}\tau\left[(n-m)\Omega_2 - p(\Omega_1+\Omega_2)\right]} d\tau \right\} \delta(p - m_1 B_1) \int_{r_h}^{r_t} J_m(k_n r \sin\theta) \\ & \times F_w W_p S_c(\sigma_p, M_r) e^{\mathrm{i}p(\varphi_w + \varphi_b)} \left(\cos\theta \sin\chi_2 - \frac{m}{k_n r} \cos\chi_2 \right) dr. \end{aligned} \tag{25}$$

The summation over index l can be performed applying Poisson summation formula

$$\sum_{l=1}^{B_2} e^{\mathrm{i}(n+p-p(\Omega_1+\Omega_2)/\Omega_2)2\pi(l-1)/B_2} = \sum_{m_2=-\infty}^{\infty} B_2 \delta(n + p - p(\Omega_1 + \Omega_2)/\Omega_2 - m_2 B_2) . \tag{26}$$

The Kronecker delta function in Eq. (26) leads to

$$n\Omega_2 = m_2 B_2 \Omega_2 + m_1 B_1 \Omega_1 . \tag{27}$$

Furthermore, the term in the curly brackets will be zero, except for

$$\frac{\Omega_2}{2\pi} \int_0^{\frac{2\pi}{\Omega_2}} e^{\mathrm{i}\tau\left[(n-m)\Omega_2 - p(\Omega_1+\Omega_2)\right]} d\tau = \delta\left[\left(n-m\right)\Omega_2 - p(\Omega_1 + \Omega_2) \right]. \tag{28}$$

Similarly, the Kronecker delta function gives rise to

$$n\Omega_2 = m_1 B_1 \Omega_1 + (m_1 B_1 + m)\Omega_2 . \tag{29}$$

Both Eqs. (27) and (29) need to be satisfied, so the Bessel function order m has to be

$$m = m_2 B_2 - m_1 B_1 . \tag{30}$$

Finally, for a single mode indexed as (m_1, m_2), Eq. (22) becomes

$$\begin{aligned} P_{m_1,m_2} = {} & \frac{\mathrm{i}B_1 B_2 k_n}{4\pi r_o} e^{\mathrm{i}k_n r_o} e^{\mathrm{i}(m_2 B_2 - m_1 B_1)(\varphi_o - \pi/2)} \int_{r_h}^{r_t} J_{m_2 B_2 - m_1 B_1}(k_n r \sin\theta) F_w W_p \\ & \times S_c(\sigma_p, M_r) \left(\cos\theta \sin\chi_2 - \frac{m_2 B_2 - m_1 B_1}{k_n r} \cos\chi_2 \right) e^{\mathrm{i}m_1 B_1 (\varphi_w + \varphi_b)} dr \end{aligned} , \tag{31}$$

where k_n becomes

$$k_n = k_{m_1,m_2} = n\Omega_2 / c_0 = (m_2 B_2 \Omega_2 + m_1 B_1 \Omega_1) / c_0 . \tag{32}$$

Consequently, the frequency for the interaction noise is calculated as

$$f_n = f_{m_1,m_2} = c_0 k_n / (2\pi) = (m_2 B_2 \Omega_2 + m_1 B_1 \Omega_1) / (2\pi) , \tag{33}$$

where the terms $B_1\Omega_1/(2\pi)$ and $B_2\Omega_2/(2\pi)$ are the **b**lade **p**assing **f**requencies (BPF) of the front and rear rotors, respectively. Then a useful expression for $k_n r$ can be evaluated as

$$k_n r = m_1 B_1 M_1 + m_2 B_2 M_2 , \tag{34}$$

where M_1 and M_2 are the rotational Mach numbers at r for the front and rear rotors, respectively. Evaluating the Bessel function at a typical radius r_e and making $\nu = k_n r_e$, we can simplify Eq. (31) into a more compact form

$$P_{m_1,m_2} = \frac{\mathrm{i}B_1 B_2}{4\pi r_o r_e} e^{\mathrm{i}m(\varphi_o - \pi/2)} e^{\mathrm{i}\nu r_o / r_e} \nu J_m(\nu \sin\theta) \left(\cos\theta T_{m_1} - \frac{m}{\nu} D_{m_1} \right), \tag{35}$$

where $T_{m_1}$and D_{m_1} are, respectively, the axial thrust and the rotating drag magnitudes of the force F induced by the p-th ($p = m_1 B_1$) inflow harmonic. Their expressions are written as

$$T_{m_1} = \int_{r_h}^{r_t} F_w W_{m_1} S_c(\sigma_{m_1}, M_r) \sin\chi_2 e^{\mathrm{i}m_1 B_1 (\varphi_w + \varphi_b)} dr , \tag{36}$$

and

$$D_{m_1} = \int_{r_h}^{r_t} F_w W_{m_1} S_c(\sigma_{m_1}, M_r) \cos\chi_2 e^{\mathrm{i}m_1 B_1 (\varphi_w + \varphi_b)} dr . \tag{37}$$

3 Discussions

In Section 2, the interaction noise radiated from CR fans has been formulated, which occurs at the frequencies composed of the integer multiples of the front rotor BPF and the rear rotor BPF. Some important features are discussed in the following, with further investigation of the formula.

3.1 Stator-rotor interaction noise

Unlike the CR fan case, the rotor BPF and its harmonics in the stator-rotor interaction problem determine the interaction frequencies completely, which will not be associated with vane numbers of the stator. Concretely speaking, with the front rotor fixed (i.e., $\Omega_1 = 0$) and for a single sound harmonic m_2, the stator-rotor interaction noise can be conveniently obtained from Eq. (35) as

$$\begin{aligned} P_{m_2} = & \sum_{m_1=-\infty}^{+\infty} \frac{\mathrm{i}B_1B_2m_2B_2\Omega_2}{4\pi r_o c_0} e^{\mathrm{i}m(\varphi_o-\pi/2)} e^{\mathrm{i}m_2B_2\Omega_2 r_o/c_o} \\ & \times J_{m_2B_2-m_1B_1}\left(m_2B_2M_2\sin\theta\right)\left(\cos\theta T_{m_1}-\frac{m}{\nu}D_{m_1}\right). \end{aligned} \tag{38}$$

It can be seen that, for the stator-rotor case, each sound harmonic m_2 contains all integer m_1 values in summation from $-\infty$ to $+\infty$, while the frequency is solely determined by the integer multiples of the rotor BPF (that is, $B_2\Omega_2/2\pi$). As for the CR case, it appears that each sound harmonic contains only one sound radiation mode (m_1, m_2), and the frequency is given by Eq. (33). However, it should be noted that the rotor-stator interaction noise cannot be obtained, at least for the present derivation, by substituting $\Omega_2 = 0$ into Equation (35), for Equation (28) is no longer valid. In fact, for CR fans the far-field observer will hear all the interaction noise occurring at angular frequencies of $|m_1B_1\Omega_1+m_2B_2\Omega_2|$, with m_1 and m_2 taking integer values from $-\infty$ to $+\infty$. The Bessel function order $m = m_2B_2-m_1B_1$ is an index of the spinning pressure mode, significantly influencing the radiation efficiency of the interaction noise. As m approaches ∞, the Bessel function vanishes rapidly, suggesting that the dominant interaction noise happens when m is small, typically $|m| \leq 3$ for small fans. Compared with the stator-rotor interaction noise, an additional term appears in the argument of the Bessel function for CR fans, that is, $z = k_n r\sin\theta = (m_1B_1M_1 + m_2B_2M_2)\sin\theta$ with $m_1B_1M_1$ being the additional term. Therefore, it tends to result in a bigger value of z, even though M is very small for small CR fans, typically $M < 0.1$. As z grows larger, the modal directivity of the interaction noise from CR fans becomes more complicated, which would

be further investigated in Sec. 4. For small computer cooling fans, the modal directivity of the rotor-strut interaction noise was studied extensively in a previous paper [22].

3.2 Interaction noise abatement strategies

With close inspection of the derived formula, some abatement strategies of interaction noise for CR fans are summarized as follows.

1. It can be seen that the most basic noise control method for small CR fans is to mismatch the front and rear rotor blade numbers, B_1 and B_2, respectively, in the purpose of generating a higher mode $m = m_2B_2 - m_1B_1$ as it manifests mathematically as the Bessel function order. The interaction noise from the net thrust force will be radiated whenever $m = 0$ (the coincident mode) and correspondingly the interaction noise from the drag force becomes zero because of the coefficient on the drag component D_{m1} in Eq. (35). Therefore, the leading modes for the thrust noise and the drag noise are respectively 0 and ±1; the zeroth mode should be carefully avoided by choosing appropriate blade numbers, especially in the low-frequency range.

2. The second noise control technique is to incorporate blade sweep based on Eqs. (5), (14) (36) and (37) in the design process because the rotor force relies upon the radial superposition of the net circumferential loads. The effect of blade sweep is anticipated to dephase the net circumferential loads from different radial sections of the blade and hence reduce noise radiation.

3. The third noise reduction measure is to increase the interstage gap between the front rotor and the rear rotor. This will result in the broader half-wake width b_w and a smaller wake centerline deficit $w(\xi_1)$ and thus reduce the unsteady lift force exerted on the rotor blades [23]. Nevertheless, such quieting measures are likely to impose weight, structure, and efficiency penalties.

4. The fourth noise reduction approach is to maintain a relatively low tip speed, which is generally useful for turbomachinery components. Based on Eq. (34), lower tip speeds will give rise to smaller arguments (z) of Bessel function. In particular, for orders other than the coincident mode ($m = 0$), the magnitude of Bessel function declines with the decrease of z within the range of $z \leq m$.

4 Modal directivity investigation

As an application and validation of the derived formula, the modal directivity patterns of the radiated interaction noise from a small CR fan are investigated, which is generally supported by the experimental results.

4.1 Experimental setup

The acoustic data generated from a small-size (116 mm in diameter) CR fan working at design point are utilized for the analysis.

Table 1 The specific parameters of the contra-rotating fan.

Parameters	Front rotor	Rear rotor
Hub radius r_h (mm)	31.5	31.5
Tip radius r_t (mm)	57.2	57.2
Duct diameter D (mm)	116	116
Tip clearance e (mm)	0.8	0.8
Axial chord length c_a (mm)	24	30
Rotational speed N (rpm)	3650	3180
Blade number B	7	5
Solidity σ	1	0.95

The testing fan is designed working at the standard atmospheric condition to deliver 3.5 m^3/min airflows with a total pressure rise of 155 Pa. In the design process of the testing fan, velocity components in the spanwise direction are determined according to simple radial equilibrium equation and by assuming a polynomial description of tangential velocity to evaluate the axial velocity numerically [24]. The profile of the blade section is chosen to be NACA 65-010 airfoil, which is stacked radially with the center of gravity of each profile as the stacking point to achieve a 3D blade. Based on the derived formula, the blade numbers of the front and rear rotors are carefully chosen to be 7 and 5, respectively, in an effort to prevent the most efficient radiation mode, namely the coincident mode m = 0, from happening in the low-frequency range. Furthermore, the interstage gap between the trailing edge of the front rotor and the leading edge of the rear rotor is axially set to be 18 mm. The detailed parameters of the designed CR fan are summarized in Table 1.

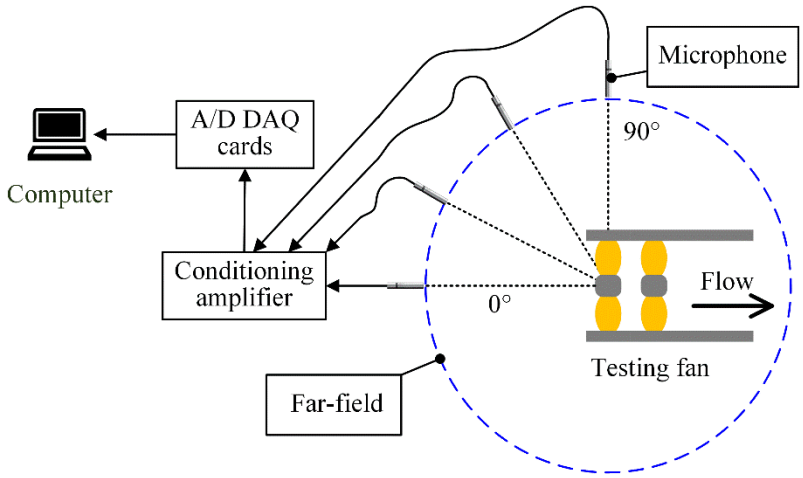

Fig. 3. Experimental setup for acoustic measurement.

The far-field acoustic experiment is organized in a fully anechoic chamber with a cutoff frequency of 100 Hz. The BPFs of the front rotor and the rear rotor are 425 Hz and 264 Hz, respectively, so the experimental environment simulates a free space. The schematic of the acoustic measurement is illustrated in Fig. 3. The testing fan is installed at the inlet of the test rig, which is built according to ANSI/AMCA Standard 210 [25] for accurate measurements of the volumetric flow rate and the total pressure rise produced by the testing fan. Four 1/4-inch microphones (BSWA), powered by a B&K Nexus conditioning amplifier (Type 2690), are evenly located at four angular positions at a distance of $r = 0.8$ m from the fan center at a height level with reference to the center. The duration for each data acquisition process at one measurement position is 20 s. The signals from the microphone are sampled by a 16-bit A/D card (NI USB-6251) at a rate of 51.2 kHz and then processed with MATLAB on a personal computer. The noise radiated into the tube of the test rig is considered to be entirely absorbed by the duct lining and does not influence the far-field noise measurement. The fan rotational speed (rev/min, *rpm*) is monitored by a tachometer, the output of which is used as the input for the Vold-Kalman (VK) multi-order filtering [26]. Note that the mean values of rotational speeds in the experiment are slightly different from those in the design process, with 3642 *rpm* and 3168 *rpm* for the front and rear rotor, respectively. The averaged sound spectrum is obtained by averaging the spectra from the four angular locations. A-weighting is applied to the measured SPL for the sake of accounting for the relative loudness perceived by the human ear. A-weighted SPL is abbreviated as SPLA, which is denoted in dBA (re. 20 μPa) in this paper.

4.2 Vold-Kalman filtering

In the study of processing fan noise, it is essential to decompose noise signal into tonal and broadband components to investigate the related modal directivity and to evaluate the efficacy of noise control strategies.

There are several methods in the literature to determine the tonal and broadband components from fan signals. A time-base-stretched synchronous method was used by Huang [27] to process the noise signal from a computer cooling fan. The spectrum of 'rotary sound' was separated from that of the raw signal, and further results showed that the change of rotational speed would cause rotary noise energy to leak into random noise energy. This method is convenient to process noise signal from a single-stage fan, of which the signal presents a strong periodicity in the time domain. However, it may mean some difficulties for CR fans because noise signals from the front rotor and the rear rotor are tightly coupled. The peak-finding algorithm is popular and has been employed by many researchers [28, 29] due to its simplicity and intuitivity. However, it is inherently subjective and not mathematically rigorous, for it requires some predefined smoothing parameters such as peak height threshold and frequency bandwidth for chopping off the tonal components. Another available method proposed by Sree has also been used to determine noise components of CR open rotors; this method works better with the front and rear rotors running at equal speeds than with unequal speeds [30, 31]. An order tracking technique known as the Vold-Kalman (VK) filter that was invented by Vold and Leuridan [26], has been recently used to filter out the harmonic noise components of fan acoustic data [32]. Pan et al. proposed an alternative VK filtering order tracking approach to extract order components of noise and vibration signals from rotary machinery in an adaptive manner [33, 34]. A two-shaft VK order tracking filter was utilized by Stephens [35] to process the sound data from CR open rotors. The results demonstrated that the order tracking filter was a robust tool for separating tonal and broadband components of a signal from CR configurations.

Therefore, in the present study, the signal processing technique based on VK multi-order filtering is employed to determine the tonal and broadband components of the acoustic data from a small CR fan. The VK multi-order filter is essentially a time-domain tracking filter and can be described by structural and data equations, which are solved as a linear least-squares problem to determine the signal components. The filter is similar to the well-known Kalman filter from the

perspective of the mathematical description. However, the filter output properties differ significantly. The VK filter behaves as a narrow bandpass filter, the center frequency of which is governed by the rotational speed of the fan. Therefore, the time-varying rotational speed and the frequency of the tracking order must be determined before filtering. The VK filter has been developed in two generations. The first generation outputs the filtered signal directly while the second generation outputs the envelope of the filtered signal at the given frequency. The second generation filter is used in this paper to process the acoustic data from a small CR fan working at the design point. Regarding the mathematical description of the second generation filter, it is well defined in Refs. [32, 35, 36]. Moreover, the technique of how to set an appropriate bandwidth for the filter is given in Ref. [36]. In this paper, in order to reduce the computing effort, multi-order tracking filtration is realized by running the single order tracking filtration repeatedly to separate the interaction tones predicted in the derived formula from the acoustic data.

4.3 Measured spectrum

Figure 4(a) shows the averaged spectrum (Ave. SPLA) of four measuring positions for the CR fan working at the design point. In the graph, the prominent tones protruding obviously from the broadband bottom with levels larger than 36 dBA are marked for illustration, where f_1 and f_2 represent the front rotor BPF and the rear rotor BPF, respectively. The prominent tones are composed of the second and third harmonics of f_2 and the interaction tones with order $|m| \leq 3$ below 3000 Hz. Hence, these tones are separated from the acoustic data with the VK filter. It should be pointed out that there are other tones protruding in the spectrum, whereas they are not separated because their levels cannot compete for the prominent ones. Table 2 lists all the separated tones, the spectra of which are demonstrated in Fig. 4b.

Table 2 The prominent tones of the designed CR fan.

f_{m_1,m_2}	$2f_2$ 528 Hz	f_1+f_2 689 Hz	$3f_2$ 792 Hz	f_1+2f_2 953 Hz	$2f_1+3f_2$ 1642 Hz	$3f_1+4f_2$ 2332 Hz
m_1	0	1	0	1	2	3
m_2	2	1	3	2	3	4
m	10	-2	15	3	1	-1

As shown in Fig. 4, the three loudest tones occur, in ascending order, at 528 Hz, 1642 Hz and 953 Hz with noise levels of 39.3 dBA, 40.4 dBA, and 42.4 dBA, respectively. The tone at 528 Hz ($2f_2$) is the second harmonic of the rear rotor BPF, while the other two are the interaction tones

with order $|m| = 1$. It seems unexpected that the tones at 528 Hz and 792 Hz are accompanied by relatively significant noise levels on account of their higher orders of the Bessel function. In essence, with $m_1 = 0$, these two tones could be ascribed to Gutin's noise [37], which, however, tends to become efficient only when the rotor tip Mach number M_t approaches to unity. With M_t in the present case being very small ($M_t < 0.1$), the tones here should not protrude very much from the broadband bottom. Therefore, it is suspected that the mechanism of the tones here is due to a different noise source, such as inflow distortion or rotor-strut interaction. It is possible that other than the steady and spatially varying parts, the incoming flow to the rear rotor has coherent turbulence structures, which are chopped periodically by the rear blades. The order of the Bessel function due to such interaction pattern is $m = m_2B_2–p$, of which p does not need to be m_1B_1 but takes integer values from $-\infty$ to $+\infty$. On the other hand, there are 11 support struts of 2mm in diameter between the front and rear rotors; as a result, the strut-rotor interaction also has a chance. In fact, the strut-rotor interaction behaves like stator-rotor interaction, producing modes $m = m_2B_2–qV$, where V is the strut number, and likewise, q takes integer values from $-\infty$ to $+\infty$. The mode orders from both mechanisms could be significantly lower than those of Gutin's noise [37], which makes the noise radiate efficiently at 528 Hz and 792 Hz. The phenomenon due to inflow distortion has also been reported by Sharma and Chen in a recent paper [38].

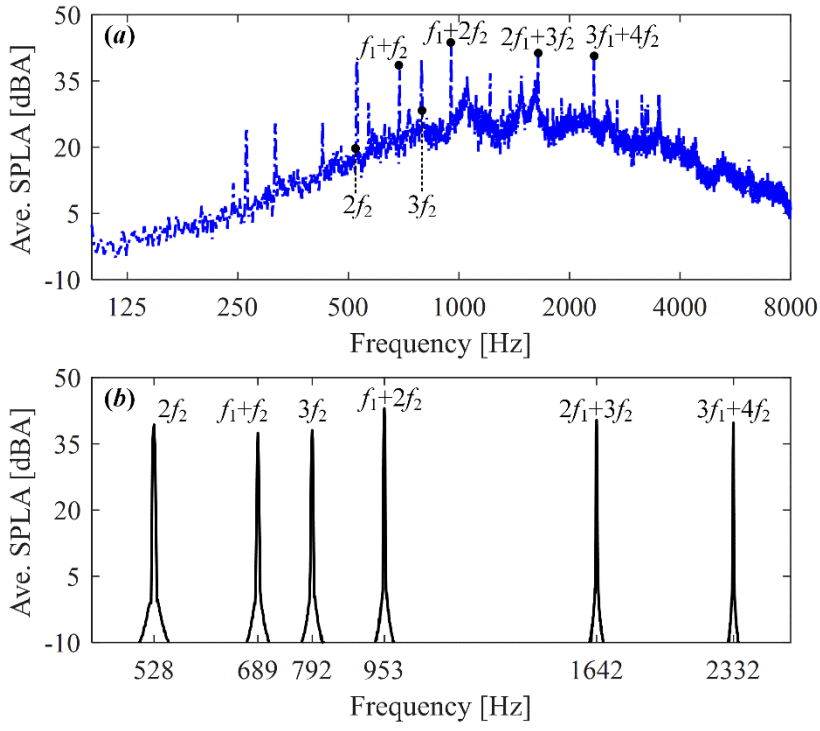

Fig. 4. The averaged spectra for (a) the raw signal and (b) the separated tones.

4.4 Modal directivity analysis of the interaction noise

The modal directivities of lower-order interaction tones are investigated, which are compared with experimental results obtained through the VK multi-order filtering method. In contrast to conventional fans, for which approximating the Bessel function by assuming v to be small is appropriate for noise analysis due to small M_t [22, 27], the noise analysis by the assumption may not be accurate for CR fans because of an additional term in the argument of the Bessel function. This additional term is expected to give more complexities in the modal directivities of the interaction noise from a CR fan, as we can see in the following.

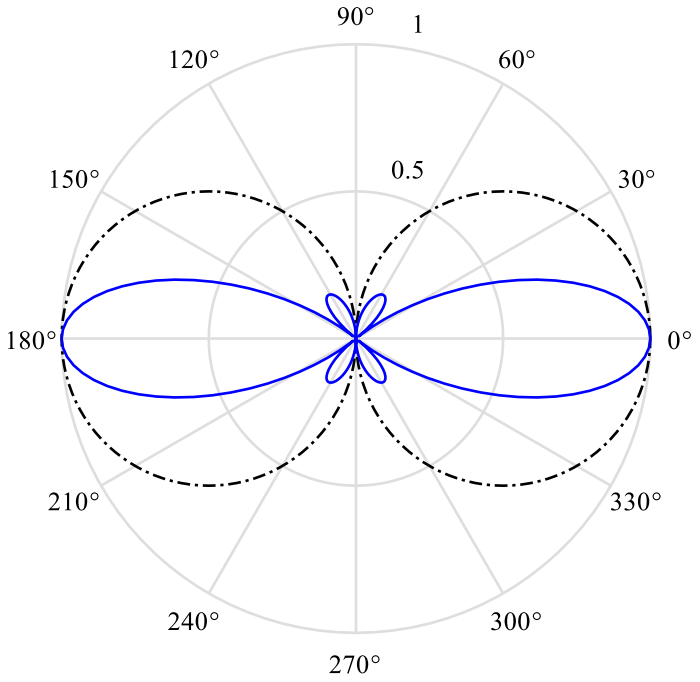

Fig. 5. Theoretical modal directivity of the $m = 0$ tone for $v \approx 0$ (— • —) and 3.79 (——).

For the mode of $m = 0$, which has been described as the coincident mode, only the thrust force T_{m_1} contributes to noise radiation, while the contribution from the drag force D_{m_1} is zero. The sound pressure of this mode is proportional to $J_0(v\sin\theta)\cos\theta$ (denoted as T0), so the leading order thrust noise peaks at $\theta = 0°$ and reaches the nadir in the rotational plane ($\theta = 90°$). Moreover, when v is small enough, $J_0(v\sin\theta) \approx 1$, T0 is reduced to $\cos\theta$. In this case, the modal directivity is a simple

dipole in the axial direction, as illustrated in Fig. 5, which is often the case for conventional fans. However, it is not necessarily true for CR fans, as v consists of two components according to Eq. (34). For the present case, v is found to be around 3.79 for the leading order thrust noise occurring at 3974 Hz, with the rotational Mach number $M \approx 0.06$ for the rear rotor. Note that both v and M are calculated at a radial location with 80% blade height. The modal directivity, in this case, is also illustrated in Fig. 5. It is found that the blue curve is much thinner than the black dashed one, indicating that the modal directivity becomes more concentrated along the rotation axis with the increase of v. Besides, the combination of $\cos\theta$ and $J_0(v\sin\theta)$ gives rise to a multi-lobe modal pattern that contains two main lobes in the axial direction as well as another four weak sub-lobes, peaking in the directions about 30° relative to the rotational plane. In the present experiment, since we have optimized the blade numbers to avoid the most efficient mode of $m = 0$, the leading order thrust noise does not obviously protrude in the averaged spectrum at 3974 Hz, which is probably masked by the broadband noise as shown in Fig. 4(a). Therefore, the VK filter is not utilized to separate this tone, and only the theoretical modal directivity of the leading thrust tone is presented.

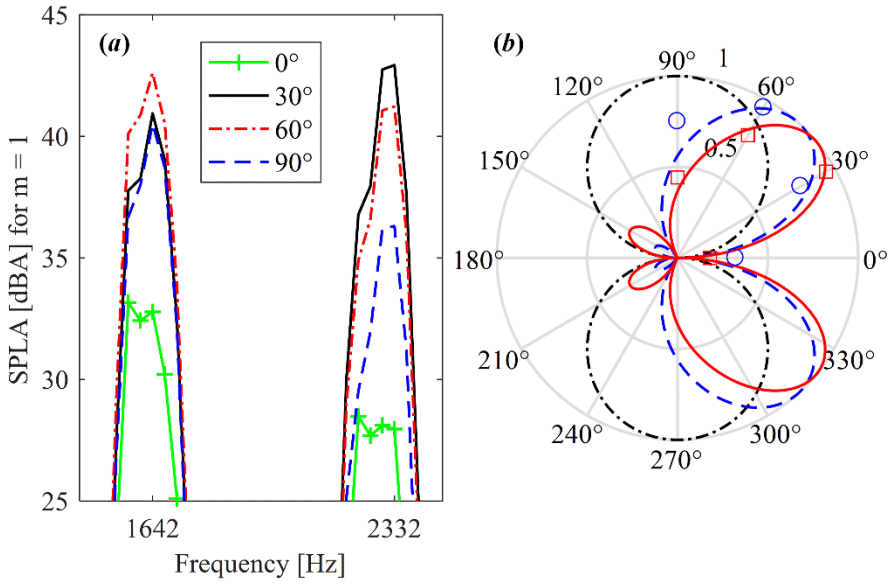

Fig. 6. The interaction tones of $|m| = 1$ order; (a) the spectrum of the extracted tones by VK filter; (b) the modal directivities for $v \approx 0$ (—•—), 1.58 (– –) and 2.25 (——).

For the mode $|m| = 1$, the thrust noise scales as $J_1(v\sin\theta)\cos\theta$ (denoted as T1), while the drag noise happens at the leading order and features $J_1(v\sin\theta)(1/v)$ (denoted as D1). According to the methodology of analyzing the modal directivity for a conventional computer cooling fan in Ref.

[24], the possible combinations of T1 and D1 are T1+D1 and T1−D1. It can be found that the combination of T1+D1 would radiate more sound forward out of the fan inlet since in this domain $\cos\theta$ and $1/v$ are addable. In contrast, the combination of T1−D1 tends to be noisier rearwards. In the experiment, due to the structural constraints of the test rig, only the acoustic directivity forward out of the fan inlet can be obtained, which will be compared with the theoretical prediction from the combination of T1 + D1. The interaction noise of mode $m = 1$ and -1 shows up at 1642 Hz and 2332 Hz, for which the corresponding v numbers can be determined as about 1.58 and 2.25, respectively. It should be noted that the modal directivity pattern can be approximated as $\sin\theta$ when v is negligibly small, which generates a drag-dominated noise (D1). When v is not tiny enough, being the case for the present CR fan, the directivity pattern may be different. The modal directivities for T1 + D1 with varying numbers of v are illustrated in Fig. 6(b) in polar plots. It can be observed that all modal patterns are symmetric with respect to the rotation axis, while the trend for $v \approx 0$ is essentially a simple dipole in the rotational plane. Different from the case of $v \approx 0$, for $v = 1.58$ and 2.25, the directivity patterns exhibit a forward-leaning characteristic, while the one for $v = 2.25$ leans even more to the rotation axis.

Using the VK filter, the two tones at 1642 Hz and 2332 Hz are extracted, the spectra of which are shown in Fig. 6(a). Both tones present their lowest noise level on the rotation axis, but the directions of maximum noise levels are different. Concretely speaking, at 1642 Hz, the largest measured sound level 42.6 dBA comes from 60°, whereas, at 2332 Hz, the peak noise level 42.9 dBA is observable at $\theta = 30°$. For the sake of validating the modal directivities predicted by the formula, the measured noise levels, at 1642 Hz (blue circle) and 2332 Hz (red square), are normalized and embedded in Fig. 6(b). By comparison, it is found that the modal directivity either at 1642 Hz or 2332 Hz has little chance to be in agreement with the prediction by assuming $v \approx 0$. Nevertheless, when the comparison is made for $v \approx 1.58$ and 2.25, the consistency is excellent, and the match is enhanced as v increases from 1.58 to 2.25.

For the mode $|m| = 2$, of which the interaction one happens at 689 Hz ($v = 0.68$), the thrust noise is proportional to $J_2(v\sin\theta)\cos\theta$ (denoted as T2), while the drag noise features $J_2(v\sin\theta)(2/v)$ (denoted as D2). Likewise, only the combination of T2 + D2 is studied. With v approaching 0, T2 + D2 manifest itself as $\sin^2\theta$ (D2), for which the noise is again dominated by the drag component. Using the VK-filter, the tone is extracted, and its spectra are given in Fig. 7(a), and the modal

directivities are shown in Fig. 7(b) with normalized noise levels (blue circle) from measurements embedded. From the spectra, it is observed that the noise levels from 0°, 30°, and 60° positions are almost the same, around 38 dBA, while the level at 90° is the lowest, about 35 dBA. The variation trend from measurements does not match well with the theoretical prediction, as shown in Fig. 7(b). This is probably because the presence of fan casing over rotors could significantly modify the directivity of the interaction tones with a higher order that peak in the rotational plane. It should also be noted that the modal directivity does not change very much as v increases from 0 to 0.68, just exhibiting a tiny forward-leaning. This characteristic could arise from the fact that the Bessel function tends to have an exponential-like feature if the argument is smaller than the order, that is, $v < m$, for which the approximation for the Bessel function by assuming $v \approx 0$ could be satisfying.

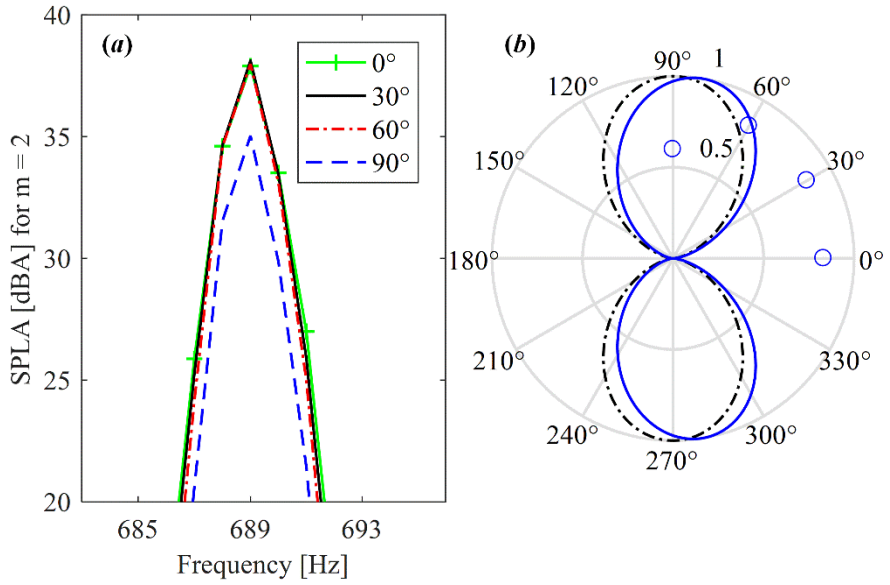

Fig. 7. The interaction tones of $|m| = 2$ order; (a) the spectrum of the extracted tones by VK filter; (b) the modal directivities for $v \approx 0$ (— • —) and 0.68 (——).

The modal directivity for $|m| = 3$ presents features similar to the mode $|m| = 2$, so it will not be discussed specifically. To summarize, the modal directivity of the interaction noise is more complicated for a CR fan than for a conventional fan. Therefore, non-negligible errors may be introduced for a CR fan analysis by simply assuming $v \approx 0$, as is the case for a traditional cooling fan.

5 Conclusion

A theoretical model is deduced to characterize the interaction noise of contra-rotating (CR) fans, and experiments have been performed to investigate the modal directivity of the interaction noise predicted from the derived model. The present work is expected to be helpful in designing quiet CR fans and devising effective noise reduction methods. The conclusions are made as below.

1. In the present model, blade section misalignments that give rise to blade sweep and lean are included during the process of modeling aerodynamic interaction between rotors, which may be helpful in designing a swept or leaned blade to dephase noise sources at different radial locations and thus to reduce noise radiation. It is obtained from the derived formula that the stator-rotor interaction noise is a special case of the present model, whereas the rotor-stator case is not. In addition, based on the derived formula, some methods of abating interaction noise are proposed, e.g., mismatching blade numbers, increasing the interstage gap between rotors and reducing rotational speeds.

2. Modal directivity of the interaction noise for a small CR fan is studied theoretically and experimentally. Compared with a conventional cooling fan, modal directivity for a CR fan is more complicated. The leading order thrust noise (coincident mode) is successfully avoided by optimizing the combination of blade number for a small CR fan. For the first-order mode, it is found that the SPLA variation trend in the θ-direction is in good agreement with that predicted from the current formula. The best agreement shows up at the frequency of 2332 Hz. In addition, the predicted directivity patterns of second- and third-order modes are dominated by the drag noise component and peak in the direction near the rotational plane.

Acknowledgments

The first author acknowledges the support from The University of Hong Kong, and China Aerodynamics Research and Development Center. The corresponding author acknowledges the fund of the Post-Doctoral Fellowship from the University of Hong Kong. This project is also supported by the National Natural Science Foundation of China (Grant No. 51775467).

References

[1] H.H. Hubbard, Sound from dual-rotating and multiple single-rotating propellers, NACA, 1948, TN No. 1654.

[2] R. Young, Contra-rotating axial flow fans, J. Inst. Heat. Vent. Eng 18 (1951) 448-477.

[3] G. Mitchell, D. Mikkelson, Summary and recent results from the NASA advanced high-speed propeller research program, AIAA/SAE/ASME 18th Joint Propulsion Conference, 1982, Ohio, AIAA-82-1119.

[4] A.J. Bradley, A study of the rotor/rotor interaction tones from a contra-rotating propeller driven aircraft, AIAA 10th Aeroacoustics Conference, 1986, Washington, AIAA-86-1894.

[5] M.J. Lighthill, On sound generated aerodynamically. I. General theory, Proc. R. Soc. Lond. A Math. Phys. Sci. 211 (1952) 564-587.

[6] D.B. Hanson, Noise of counter-rotation propellers, J. Aircr. 22 (1985) 609-617.

[7] A.B. Parry, Theoretical prediction of counter-rotating propeller noise, Ph.D. Dissertation, University of Leeds, 1988.

[8] S. Fujii, H. Nishiwaki, K. Takeda, Noise and performance of a counter-rotation propeller, J. Aircr. 23 (1986) 719-724.

[9] F.B. Metzger, P.C. Brown, Results of acoustic tests of a prop-fan model, J. Aircr. 25 (1988) 653-658.

[10] R.P. Woodward, Noise of a model high-speed counterrotation propeller at simulated takeoff/approach conditions (F7/A7), AIAA 11th Aeroacoustics Conference, 1987, California, AIAA-87-2657.

[11] H.W. Shin, C.E. Whitfield, D.C. Wisler, Rotor-rotor interaction for counter-rotating fans, part I: three-dimensional flowfield measurements, Aiaa J. 32 (1994) 2224-2233.

[12] N. Peake, A.B. Parry, Modern challenges facing turbomachinery aeroacoustics, Annu. Rev. Fluid Mech. 44 (2012) 227-248.

[13] R. Schnell, Experimental and numerical investigation of blade pressure fluctuations on a CFK-bladed, counterrotating propfan, ASME Turbo Expo 2001, 2001, Louisiana, 2001-GT-0298.

[14] T. Lengyel, C. Voß, T. Schmidt, E. Nicke, Design of a counter-rotating fan—An aircraft engine technology to reduce noise and CO_2-emissions, 19th ISABE Conference, 2009, Montreal, Canada, ISABE 2009-1267.

[15] V. Blandeau, Aerodynamic broadband noise from contra-rotating open rotors, Ph.D. Dissertation, University of Southampton, 2011.

[16] E. Envia, Open rotor aeroacoustic modeling, NASA, 2012, TM—2012-217740.

[17] J.E. Ffowcs Williams, D.L. Hawkings, Sound generation by turbulence and surfaces in arbitrary motion, Proc. R. Soc. Lond. A Math. Phys. Sci. 264 (1969) 321-342.

[18] W.K. Blake, Mechanics of flow-induced sound and vibration, Volume 2 Complex flow-structure interactions, Academic Press, Florida, 1986.

[19] C. Wang, L.X. Huang, Theoretical Acoustic Prediction of the Aerodynamic Interaction for Contra-Rotating Fans, Aiaa J. 56 (2018) 1855-1866.

[20] M.E. Goldstein, Aeroacoustics, McGraw-Hill, Inc., United States of America, 1976.

[21] I.S. Gradshteyn, I.M. Ryzhik, Table of integrals, series, and products, seventh ed., Academic Press, California, 2007.

[22] L.X. Huang, Characterizing computer cooling fan noise, J. Acoust. Soc. Am. 114 (2003) 3189-3200.

[23] B. Reynolds, B. Lakshminarayana, Characteristics of lightly loaded fan rotor blade wakes, NASA, 1979, NASA-CR-3188.

[24] T. Wright, P. Gerhart, Fluid machinery: application, selection, and design, CRC Press, Florida, 2009.

[25] AMCA, AMCA 210 Laboratory methods of testing fans for aerodynamic performance rating, American Society of Heating, Refrigerating and Air-Conditioning Engineers, Washington, 1999.

[26] H. Vold, J. Leuridan, High-resolution order tracking at extreme slew rates using Kalman tracking filters, Shock and Vibration 2 (1995) 507-515.

[27] L.X. Huang, J. Wang, Acoustic analysis of a computer cooling fan, J. Acoust. Soc. Am. 118 (2005) 2190-2200.

[28] M. Kingan, V. Blandeau, B. Tester, P. Joseph, A. Parry, Relative importance of open rotor tone and broadband noise sources, 17th AIAA/CEAS Aeroacoustics Conference, 2011, Oregon, AIAA 2011-2763.

[29] N. Liu, Characterization and control of small axial-flow fan noise, Ph.D. Dissertation, The University of Hong Kong, 2018.

[30] D. Sree, A novel signal processing technique for separating tonal and broadband noise components from counter-rotating open-rotor acoustic data, Int. J. Aeroacoust. 12 (2013) 169-188.

[31] D. Sree, D.B. Stephens, 2016. Improved separation of tone and broadband noise components from open rotor acoustic data. Aerospace. 3, aerospace3030029.

[32] A. Truong, D. Papamoschou, Harmonic and broadband separation of noise from a small ducted fan, 21st AIAA/CEAS Aeroacoustics Conference, 2015, AIAA-2015-3282.

[33] M.C. Pan, C.X. Wu, Adaptive Vold-Kalman filtering order tracking, Mech. Syst. Signal Proc. 21 (2007) 2957-2969.

[34] M.C. Pan, W.C. Chu, D.D. Le, Adaptive angular-velocity Vold-Kalman filter order tracking - Theoretical basis, numerical implementation and parameter investigation, Mech. Syst. Signal Proc. 81 (2016) 148-161.

[35] D.B. Stephens, H. Vold, Order tracking signal processing for open rotor acoustics, J. Sound Vib. 333 (2014) 3818-3830.

[36] J. Tuma, Vehicle gearbox noise and vibration: measurement, signal analysis, signal processing and noise reduction measures, John Wiley & Sons, West Sussex, United Kingdom, 2014.

[37] L. Gutin, On the sound field of a rotating propeller, NACA, 1948, TM No. 1195.

[38] A. Sharma, H.N. Chen, Prediction of aerodynamic tonal noise from open rotors, J. Sound Vib. 332 (2013) 3832-3845.